time was spent in the many gradient descent optimizations initiated in the process. In our implementation, the tree annealing optimization serves in a limited way in that the tree structure described in [5] does not become very large. However, tree annealing is still effective in determining starting points for quasi-Newton optimizations and each minimum is evaluated at approximately the cost of a single quasi-Newton optimization.

References

[1] M.-K. Vai and S. Prasad, "Computer-aided design of monolithic MESFET distributed amplifiers," *IEEE Trans. Microwave Theory Tech.*, vol. 38, no. 4, pp. 345–349, Apr. 1990.

[2] M.-K. Vai, S. Prasad, N. C. Li, and F. Kai, "Modeling of microwave semiconductor devices using simulated annealing optimization," *IEEE Trans. Electron Devices*, vol. ED-36, pp. 761–762, Apr. 1989.

[3] M.-K. Vai, J.-S. Lin, and S. Prasad, "Acceleration of simulated annealing and its application to microwave device and circuit optimization," *IEEE MTT-S Int. Microwave Symp. Dig.*, June 1991, pp. 1213–1216.

[4] S. Kirkpatrick, C. Gelatt, and M. Vecchi, "Optimization by simulated annealing," *Science*, vol. 220, pp. 671–680, May 13, 1983.

[5] G. L. Bilbro, M. B. Steer, R. J. Trew, C. R. Chang, and S. G. Skaggs, "Extraction of the parameters of equivalent circuits of microwave transistors using tree annealing," *IEEE Trans. Microwave Theory Tech.*, vol. 38, 1990, pp. 1711–1718.

[6] A. Materka and T. Kacprzak, "Computer calculation of large-signal GaAs amplifier characteristics," *IEEE Trans. Microwave Theory Tech*, vol. MTT-33, Feb. 1985, pp. 129–135.

[7] J. Gerber and R. Gilmore, "Parameter extraction of MESFETS for use in oscillator design," in *1989 WESCON/89 Conf. Rec.*, pp. 83–87.

Quasi-Static Analysis of Shielded Microstripline by a Modified Boundary Element Method

T. N. Chang and Y. T. Lin

***Abstract*—This paper presents a modified boundary element method for analyzing the shielded microstrip-like structure. The boundary integral equations are derived via the Green's second identity with the adjoint fields chosen to satisfy the boundary conditions along the outside shielding conductor. Numerically, these result in a considerably reduced matrix size compared to that using free space Green's functions as the adjoint fields. The computation time for off-diagonal element of the matrix can be decreased by taking the Maclaurin series expansion forms of the infinite sums. Results for microstrip line are found in good agreement with those in the literature.**

I. Introduction

The boundary element method has previously been applied to the analysis of lines in a shielding box with and without a dielectric substrate [1]–[2]. An analysis of microstrip line with finite thickness was presented in [3]. In this method, the wave equation is converted to an integral over the boundary of the region of interest by way of Green's second identity. Although the free space Green's function is chosen as the adjoint field in [1]–[3], it is by no means the only choice. In [4], the Green's function for the classical image problem was employed. For a shielded structure, a unified approach to determine the required Green's function was suggested [5].

One disadvantage of the choice of free space Green's function is that the matrix size formulated by discretizing the boundary integral equation is generally large since the whole shielding conductor should be discretized [3]. In this paper, a modified boundary element method is presented wherein the Green's function is forced to satisfy the boundary conditions along the shielding boundary. A boundary integral results which is performed merely along the line where the strip is located. Therefore, the required memory size will largely be reduced. This newly adopted Green's function involves a slowly-convergent infinite series. However, the computation time is reduced by application of the geometric-series method [6].

Manuscript received June 5, 1992; revised October 30, 1992. This work was supported by the Tatung Company, Taipei, Taiwan Republic of China.

The authors are with Tantung Institute of Technology, 40 Chungshan North Road, 3rd Sec., Taipei, Taiwan 10451, Republic of China.

IEEE Log Number 9206288.

II. Formulation

The cross-section of a microstripline shielded by a perfect conductor is considered. The subdomain S_i with contour $\Gamma_i\ (i = 1, 2)$ is homogeneously filled with a loss-free dielectric medium. Inside each region S_i, Laplace's equation

$$\nabla^2 \phi_i = 0 \tag{1}$$

holds, where ϕ_i denotes the electrostatic potential. Green's second identity over S_i can be expressed as

$$\iint [\varphi_i(\nabla^2 \phi_i) + \phi_i(\nabla^2 \varphi_i)] ds_i = \int [\varphi_i(\partial \phi_i / \partial n_i) - \phi_i(\partial \varphi_i / \partial n_i)]\, d\Gamma_i \tag{2}$$

where φ_i is a suitable adjoint field and $\partial/\partial n_i$ the derivative in the positive normal direction. The free space Green's function is chosen for φ_i in [1]–[3] for boundary element formulation. The disadvantage of this choice is that the boundary integral equation must be performed on both contours $\Gamma_1\ (= ABCDEFA)$ and $\Gamma_2\ (= ABCGHFA)$. There results in a large memory size if the boundary scale is considerably large. In this paper, each Γ_i is divided into two parts Γ_i^g and Γ_i^r, where the superscript g and r stand for the ground and the remainder parts respectively. For example, we have $\Gamma_1^g = CDEF$ and $\Gamma_1^r = FABC$. The suitable adjoint field φ_i now can be chosen to satisfy the required boundary condition on the ground plane. In the present case, the Green's function for a rectangular trough region [6] was chosen as the candidate. With the coordinates shown in Fig. 2, two Green's functions for the homogeneous rectangular trough regions are needed. They satisfy the following differential equations:

$$[\partial^2 \varphi_i / \partial x^2] + [\partial^2 \varphi_i / \partial y^2] = -(1/\epsilon_i)\delta(x - x_i)\delta(y - y_i) \quad i = 1, 2 \tag{3a}$$

where δ is the Dirac Delta function, $\epsilon_1 = \epsilon_0 \epsilon_r, \epsilon_2 = \epsilon_0$, and (x_i, y_i) is the source point in the ith region.

To facilitate understanding, φ_i is given by

$$\varphi_i(x, y/x_i, y_i) = (2/\pi\epsilon_i) \sum_{n=1}^{\infty} (1/n) \sin(n\pi x_i/b) \sin(n\pi x/b) \cdot \sinh[(n\pi/b) f_i] \exp[(n\pi/b) g_i] \tag{3b}$$

where $(f_1, g_1) = (y_1, -y)$ for $y > y_1$; $(f_1, g_1) = (y, -y_1)$ for $y \le y_1$; $(f_2, g_2) = (h + h' - y, y_2 - h - h')$ for $y > y_2$; and $(f_2, g_2) = (y_2 - h - h', y - h - h')$ for $y \le y_2$).

Note that $\phi_i = 0$ along the ground part in each region. Judging from the right-hand side of (2), the boundary integral path can now be performed merely on the remainder (the interface plane) part. Therefore, the memory size will largely be reduced.

Equation (2) can be put in the following matrix form once φ_i is obtained and Γ_i' is divided into M segments in each region.

$$[A_i]_{M\times M}[\phi_i]_{M\times 1} = [B_i]_{M\times M}[\partial\phi_i/\partial n_i]_{M\times 1} \tag{4}$$

where $[\phi_i] = [\phi_i^1, \phi_i^2, \cdots, \phi_i^p, \cdots, \phi_i^M]^T$ and $[\partial\phi_i/\partial n_i] = [\partial\phi_i^1/\partial n_i, \partial\phi_i^2/\partial n_i, \cdots, \partial\phi_i^p/\partial n_i, \cdots, \partial\phi_i^M/\partial n_i]^T$ respectively represents the column matrix ($i = 1, 2$) with ϕ_i^p and $\partial\phi_i^p/\partial n_i$ ($p = 1, 2, \cdots, M$) the values of the potential and its normal derivative at the nodal point of the pth element. Denoting the elements of $[A_i]_{M\times M}$ and $[B_i]_{M\times M}$ by A_i^{pq} and B_i^{pq}, the elements mainly involve the following computations

$$\sum_{n=1}^{\infty} \mathrm{csn}\,(n\xi)/n \quad \text{and} \quad \sum_{n=1}^{\infty} \mathrm{csn}\,(n\xi)/n^2 \tag{5}$$

where csn represents sin or cos function, ξ is the normalized x-coordinate with $0 < \xi < 2\pi$. For example,

$$A_1^{pq} = \left(4/\pi\right)\sum_{n=1}^{\infty}(1/n)\sin(n\pi x_p/b) \cdot \exp(-n\pi h/b)\cosh(n\pi h/b) \cdot \left[\cos\left(n\pi x_q^+/b\right) - \cos\left(n\pi x_q^-/b\right)\right] \quad (p \neq q) \tag{6a}$$

$$A_1^{pp} = 1 \tag{6b}$$

where (x_p, h) and (x_q, h) are the coordinates of nodal points of the pth and qth elements respectively. $x_q^+ = x_q + (w_q/2)$ and $x_q^- = x_q - (w_q/2)$, with w_q the width of the qth element.

Following the procedures in [3], we can obtain the final boundary matrix equation in the form

$$[A][X] = [B] \tag{7}$$

where $[A]$ is a $2M\times 2M$ matrix, $[X]$ contains the unknown quantities, and $[B]$ is the known right-hand vector. Note that Γ_i' is divided into M segments in each region. The infinite sums in (6a) can be simplified by the geometric-series method of reference [6]. For example, (6a) is changed into:

$$A_1^{pq} = (2/\pi)\sum_{n=1}(1/n)\Big[\sin(n\pi x_p/b)\cos\left(n\pi x_q^-/b\right) - \sin(n\pi x_p/b)\cos\left(n\pi x_q^+\right)/b\Big] \cdot \exp(-2n\pi h/b) \tag{8}$$

In this form, the sums are typically convergent within three digits by taking less than 5 terms. Therefore, the computation time for each off-diagonal element calculation is compatible with that for off-diagonal element calculation formulated using the free space Green's function. In the later case, calculation time is saved by use of four-points Gaussian quadrature [2] or by way of pulse expansion with the integrals solved analytically. However, the overall calculation time is considerably larger since the required matrix size is much larger than that in the present method.

The concept shown here is rather general. Many cases can be treated simply by modifying the adopted Green's function. For example, symmetry conditions may be applied in deriving the even or odd mode Green's function satisfying $\partial\varphi_i/\partial n = 0$ or $\varphi_i = 0$ in the symmetrical plane while applying (2). Finite metallization thickness can also be treated with a modified boundary contour as suggested in [3].

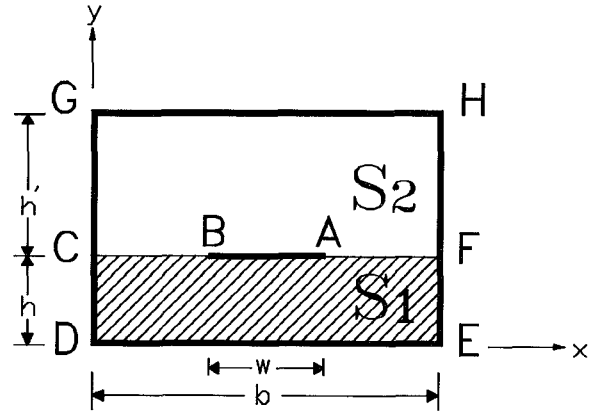

Fig. 1. Cross section of a shielded microstrip line.

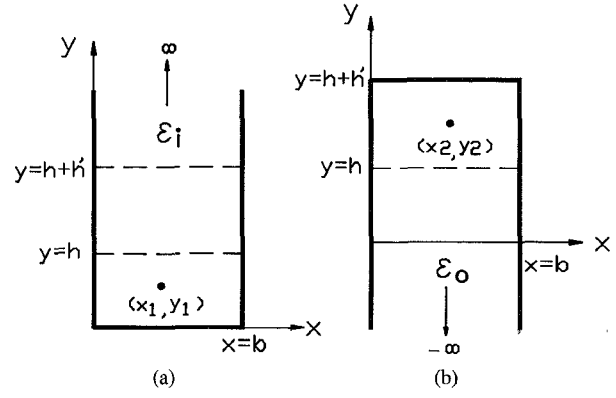

Fig. 2. Line source in a rectangular trough region. (a) For region 1. (b) For region 2.

TABLE I
COMPARISON OF CHARACTERISTIC IMPEDANCE (Z_o) AND NORMALIZED GUIDED WAVELENGTH VALUES WITH RESULTS OBTAINED BY OTHER METHOD (DIMENSIONS IN MILS, $b = 20h + w, h' = 10h$)

w	h	ϵ_r	Z_o [7]	λ_g/λ_o [7]	Z_o this method		λ_g/λ_o this method	
					($t = 1$)	($t = 2$)	($t = 1$)	($t = 2$)
10	67	2.9	165.9	0.693	168.9	166.8	0.694	0.693
15	14	4.7	67.2	0.546	68.5	67.6	0.549	0.547
22	19	4.3	67.2	0.567	68.5	67.2	0.569	0.568
20	31	4.7	84.4	0.554	86.6	84.2	0.553	0.553

III. NUMERICAL RESULTS

Analysis of microstripline has been presented in the literature extensively. For the simple structure shown in Fig. 1, calculations by the present method are listed in Table I. As EM theory shows that fields vary rapidly near strip-conductor edges. The adoption of nonuniform discretization was also studied. We symmetrically bisect the strip, and divide each half strip into p segments. Assume that the width of the segment nearest to the strip edge is s and the ratio of the width of any two neighboring segments is t. we have $s = w(1-t)/[2(1-t^p)]$ for $t > 1$and $s = w/2p$ for $t = 1$. In our calculations, AB was divided into 14 segments, while BC and AF were divided into 14 segments individually. Comparing to [7], it is noted from Table I that results by nonuniform discretization (choose $t = 2$) have more good agreement.

IV. CONCLUSION

A new modified boundary element method is applied to the analysis of shielded microstripline. The new method is based on

the choice of an adjoint field which satisfies part of the required boundary conditions. In the numerical analysis, the resulting matrix is considerably reduced (for example, compared with [3]). The computation time is also largely reduced by taking the Maclaurin series expansion forms of the infinite sums.

The formulation shown here is rather general. It can in principle be applied to various structures involving inhomogeneous dielectric media (e.g., multiconductor transmission lines in multilayered dielectric media). Finite metallization thickness can also be considered with a modified choice of the contour as already suggested in [3].

REFERENCES

[1] T. Honma and I. Fukai, "An analysis for the equivalence of boxed and shielded strip lines by a boundary element method," *Trans. IECE Japan,* vol. J65-B, pp. 497–498, 1982.

[2] M. Ikeuchi, "Boundary element analysis of shielded microstrip lines with dielectric layers," *Trans. IECE Japan,* vol. J67-E, no. 11, pp. 585–590, 1984.

[3] T. N. Chang and C. H. Tan, "Analysis of a shielded microstrip line with finite metallization thickness by the boundary element method," *IEEE Trans. Microwave Theory Tech.,* vol. 38, no. 8, pp. 1130–1132, 1990.

[4] V. Postoyalko, "Green's function treatment of edge singularities in the quasi-TEM analysis of microstrip," *IEEE Trans. Microwave Theory Tech.,* vol. 34, no. 11, pp. 1092–1095, 1986.

[5] B. Bhat and S. K. Koul, "Unified approach to solve a class of strip and microstrip-like transmission lines," *IEEE Trans. Microwave Theory Tech.,* vol. 30, no. 5, pp. 679–685, 1982.

[6] R. E. Collin, *Field Theory of Guided Waves* New York: McGraw-Hill, 1960, pp. 52–54, pp. 576–581.

[7] T. Itoh, "A method for analyzing shielded microstrip lines," *Trans IECE, Japan,* vol. j58-B, pp. 24–29, Jan. 1975.

CAD of T-Septum Waveguide Evanescent-Mode Filters

Vladimir A. Labay and Jens Bornemann

***Abstract*— This paper presents a mode-matching-based design of evanescent-mode waveguide filters with T-septum shaped metal inserts. Owing to the wideband characteristics of the T-septum waveguide, the proposed design constitutes a significant improvement over common evanescent-mode filters with respect to both size reduction and stopband behavior. The theoretical approach is verified at the example of a three-resonator 8.8-GHz filter prototype of less than 3/4 inch length. The second passband is beyond 27 GHz. Since the design procedure takes higher-order mode interactions into account, good agreement between theory and experiment is obtained over the entire measurement range between 8.2 and 40 GHz.**

I. INTRODUCTION

Evanescent-mode filters are constructed from resonators within a below-cutoff waveguide section and rectangular waveguide discontinuities for connection to a standard-size input/output guide [1]–[5]. The resonators are formed by introducing appropriate obstacles such as capacitive screws [1], round posts [2], dielectric blocks [3], ridges [4] or E-plane fins [5] at suitable intervals along the below-cutoff section. While in a given frequency band, the filter response improves with reducing the size of the evanescent-mode guide, two problems are immediately associated with the resonators of such filters. First, their cross-sections need to be specifically shaped in order to allow for a considerable reduction in cutoff frequency and, secondly, simplicity in shape must be maintained to apply efficient computer-aided modelling and design procedures. A structure, which satisfies these requirements but has not yet been used in evanescent-mode configurations, is the T-septum waveguide, e.g., [6].

Therefore, this paper focuses on the computer-aided design of T-septum waveguide evanescent mode filters. By incorporating the T-septum eigenfunctions [7] into a mode-matching-based design routine [8], higher-order mode interactions at all discontinuities are included, thus resulting in close agreement between predicted and measured filter responses. Another advantage of this design is its remarkably small size.

Manuscript received March 30, 1992; revised August 10, 1992.

The authors are with the Laboratory for Lightwave Electronics, Microwaves and Communications (LLiMiC), Department of Electrical and Computer Engineering, University of Victoria, Victoria, BC, Canada VPW 3P6.

IEEE Log Number 9206287.

II. THEORY

The mode-matching technique is applied to calculate the generalized scattering matrix of the T-septum waveguide evanescent-mode filter. The electromagnetic field in each longitudinal filter section is derived from the z-components of the magnetic and electric vector potential. Since the method of analysis together with the potential and eigenfunctions of the rectangular waveguide sections are already given in [8], only the T-septum waveguide cross-section functions need to be presented here. Choosing the subregion division of the cross-section according to Fig. 1 and applying electric and magnetic wall symmetry at $y = 0$ and $x = a/2$, respectively, the cross-section functions yield:

$$T_h(x,y) = \sum_{l=0}^{L-1} A_l^I \frac{\sin\left\{k_{xl}^I\left(x-\frac{a}{2}\right)\right\}}{k_{xl}^I} \frac{\cos\left\{\frac{l\pi}{b_1}y\right\}}{\sqrt{1+\delta_{0l}}} + \sum_{m=0}^{M-1} A_m^{II} \cos\{k_{xm}^{II}x\} \frac{\cos\left\{\frac{2m\pi}{b}y\right\}}{\sqrt{1+\delta_{0m}}} + \sum_{n=0}^{N-1} A_n^{III} \cos\{k_{xn}^{III}(x-a_2)\} \frac{\cos\left\{\frac{n\pi}{b-b_2}(y-b_2)\right\}}{\sqrt{1+\delta_{0n}}} \tag{1}$$

$$T_e(x,y) = \sum_{l=1}^{L-1} D_l^I \cos\left\{k_{xl}^I\left(x-\frac{a}{2}\right)\right\} \sin\left\{\frac{l\pi}{b_1}y\right\} + \sum_{m=1}^{M-1} D_m^{II} \frac{\sin\{k_{xm}^{II}x\}}{k_{xm}^{II}} \sin\left\{\frac{2m\pi}{b}y\right\} + \sum_{n=1}^{N-1} D_n^{III} \frac{\sin\{k_{xn}^{III}(x-a_2)\}}{k_{xn}^{III}} \sin\left\{\frac{n\pi}{b-b_2}(y-b_2)\right\} \tag{2}$$

Amplitude coefficients A^i, D^i and separation constants $k_x^i (i \in [I, II, III])$ are determined by the solution of the characteristic matrix equation [7] and subsequent power normalization [8]. The generalized scattering matrix of the overall structure is obtained by cascading the individual scattering matrices of the discontinuities and homogeneous sections involved, e.g., [8]. Sufficient convergence behavior is obtained with 35 TE and TM modes, $M = 20$ expansion